Title

Nucleoside diphosphate kinases fuel dynamin superfamily proteins with GTP for membrane remodeling

Journal

Science, 344(6191)

ISSN

0036-8075

Authors

Boissan, Mathieu
Montagnac, Guillaume
Shen, Qinfang
et al.

Publication Date

2014-06-27

DOI

10.1126/science.1253768

Peer reviewed

Published in final edited form as:
Science. 2014 June 27; 344(6191): 1510–1515. doi:10.1126/science.1253768.

Nucleoside diphosphate kinases fuel dynamin superfamily proteins with GTP for membrane remodeling

Mathieu Boissan[1,2,3,4,*], **Guillaume Montagnac**[1,2,†], **Qinfang Shen**[5], **Lorena Griparic**[5], **Jérôme Guitton**[6,7], **Maryse Romao**[1,8], **Nathalie Sauvonnet**[9], **Thibault Lagache**[10], **Ioan Lascu**[11], **Graça Raposo**[1,8], **Céline Desbourdes**[12,13], **Uwe Schlattner**[12,13], **Marie-Lise Lacombe**[3,4], **Simona Polo**[14,15], **Alexander M. van der Bliek**[5], **Aurélien Roux**[16], and **Philippe Chavrier**[1,2,*]

[1]Institut Curie, Research Center, Paris, France [2]Membrane and Cytoskeleton Dynamics, CNRS UMR 144, Paris, France [3]Université Pierre et Marie Curie, University Paris 06, Paris, France [4]Saint-Antoine Research Center, INSERM UMR-S 938, Paris, France [5]Department of Biological Chemistry, David Geffen School of Medicine at University of California, Los Angeles, Los Angeles, CA, USA [6]Hospices Civils de Lyon, Pierre Bénite, France [7]Université de Lyon, Lyon, France [8]Structure and Membrane Compartments, CNRS UMR 144, Paris, France [9]Institut Pasteur, Unité de Biologie des Interactions Cellulaires, Paris, France [10]Quantitative Image Analysis Unit, Institut Pasteur, Paris, France [11]Institut de Biochimie et Génétique Cellulaires-CNRS, Université Bordeaux 2, Bordeaux, France [12]Université Grenoble Alpes, Laboratory of Fundamental and Applied Bioenergetics, Grenoble, France [13]Inserm, U1055, Grenoble, France [14]IFOM, Fondazione Istituto FIRC di Oncologia Molecolare, Milan, Italy [15]Dipartimento di Scienze della Salute, Universita' degli Studi di Milano, Milan, Italy [16]Biochemistry Department, University of Geneva, & Swiss National Center for Competence in Research Program Chemical Biology, Geneva, Switzerland

Abstract

Dynamin superfamily molecular motors use guanosine triphosphate (GTP) as a source of energy for membrane-remodeling events. We found that knockdown of nucleoside diphosphate kinases (NDPKs) NM23-H1/H2, which produce GTP through adenosine triphosphate (ATP)–driven conversion of guanosine diphosphate (GDP), inhibited dynamin-mediated endocytosis. NM23-H1/H2 localized at clathrin-coated pits and interacted with the proline-rich domain of dynamin. In vitro, NM23-H1/H2 were recruited to dynamin-induced tubules, stimulated GTP-loading on dynamin, and triggered fission in the presence of ATP and GDP. NM23-H4, a mitochondria-specific NDPK, colocalized with mitochondrial dynamin-like OPA1 involved in mitochondria

[*]Corresponding author. mathieu.boissan@inserm.fr (M.B.); philippe.chavrier@curie.fr (P.C.).
[†]Present address: Institut Gustave Roussy, Inserm U1009, Villejuif, France

SUPPLEMENTARY MATERIALS
www.sciencemag.org/content/344/6191/1510/suppl/DC1
Materials and Methods
Supplementary Text
Figs. S1 to S11
References (*22*–*33*)
Movies S1 to S3

Europe PMC Funders Author Manuscripts

inner membrane fusion and increased GTP-loading on OPA1. Like OPA1 loss of function, silencing of NM23-H4 but not NM23-H1/H2 resulted in mitochondrial fragmentation, reflecting fusion defects. Thus, NDPKs interact with and provide GTP to dynamins, allowing these motor proteins to work with high thermodynamic efficiency.

Europe PMC Funders Author Manuscripts

The 100-kD dynamin guanosine triphosphatase (GTPase) promotes uptake of cell-surface receptors both by clathrin-dependent and -independent pathways (1, 2). Dynamin polymerizes into helix around the neck of endocytic pits and induces guanosine triphosphate (GTP) hydrolysis–driven membrane fission (3–7). Typical of molecular motors, dynamin has a low affinity for GTP and a high basal GTP-hydrolysis rate, which can be further stimulated by dynamin polymerization (8, 9). This maximizes chemical energy gain and kinetics of hydrolysis, respectively, which in vivo depend on high concentration ratios of adenosine triphosphate/adenosine diphosphate (ATP/ADP) or GTP/guanosine diphosphate (GDP). The cellular concentrations of GTP and GDP are at least a factor of 10 lower than those of ATP and ADP, and GTP/GDP ratios could thus decrease much more rapidly at elevated workload, both of which make GTP not an ideal substrate for high-turnover, energy-dependent enzymes. Paradoxically, dynamin GTPases are among the most powerful molecular motors described (7).

Studies in *Drosophila* identified a genetic interaction between dynamin and *Awd* (10–12). Awd belongs to the family of nucleoside diphosphate kinases (NDPKs), which catalyze synthesis of nucleoside triphosphates, including GTP, from corresponding nucleoside diphosphates and ATP (13). The most abundant human NDPKs are the highly related cytosolic proteins NM23-H1 and -H2. NM23-H4, another NDPK-family member, localizes exclusively at the mitochondrial inner membrane (14, 15). Mitochondrial membrane dynamics require dynamin-related GTPases (16). We hypothesized that NDPKs could influence the function of dynamin family members in membrane-remodeling events through spatially controlled GTP production and availability.

Knockdown of NM23-H1 and -H2 (fig. S1, A to E) reduced clathrin-dependent endocytosis of the transferrin (Tf) and epidermal growth factor (EGF) receptors (Fig. 1, A and B, and fig. S2, A to E) and clathrin-independent dynamin-dependent endocytosis of interleukin-2 receptor β subunit (Fig. 1C). The endocytic defect of EGF receptor was partially rescued by expression of wild-type, small interfering RNA (siRNA)–resistant NM23-H1, but not by kinase-dead NM23-H1^{H118N} mutant (Fig. 1D). Thus, the function of Awd/NM23 in dynamin-mediated endocytosis is conserved from *Drosophila* to mammalian cells [(10) and this study].

Like in dynamin-null cells (17), NM23-H1/H2 depletion increased the density of clathrin-coated pits (CCPs) at the plasma membrane (Fig. 2, A and B, and fig. S3, A and B). Silencing of NM23-H1/H2 led to the accumulation of deeply invaginated CCPs, in contrast to control cells, where CCPs were rarely detected at the plasma membrane (Fig. 2, C to F). Scoring for Tf-positive CCPs and vesicles in the vicinity of the plasma membrane revealed an approximately threefold augmentation in the absence of NM23 (Fig. 2G), similar to the phenotype reported in dynamin-null cells (17), suggesting a role for NM23-H1/H2 in dynamin-mediated membrane fission at CCPs.

We examined the intracellular distribution of NM23-H1/H2 and confirmed that both isoforms were predominantly cytosolic, although a low but reproducible association of both isoforms with membranes was found (fig. S4, A and B). Total internal reflection fluorescence (TIRF) microscopy analysis of cells labeled with antibody to NM23-H2 revealed the colocalization of NM23-H2 with AP-2 (α-adaptin) and dynamin-2 at CCPs (fig. S5, A to D), which was confirmed by means of proximity ligation assay (PLA), which showed a close proximity of NM23-H1/H2 with α-adaptin and dynamin-2 at CCPs (Fig. 2, H and I, and figs. S6 and S7). Furthermore, NM23-H1/H2 coimmunoprecipitated with dynamin-1 (Fig. 3A) and with dynamin-2 (Fig. 3B), and purified full-length recombinant NM23-H2 and dynamin-2 interacted directly in vitro (Fig. 3C). We investigated the contribution of the C-terminal proline-rich domain (PRD) of dynamin-2 to this interaction because this domain binds to several dynamin regulators and effectors (18). The dynamin-2 PRD domain fused to glutathione *S*-transferase (GST) pulled-down NM23-H1 and -H2, indicating that dynamin-2 physically interacts with both NM23-H1/H2 isoforms through its PRD (Fig. 3D). Thus, NM23-H1/H2 interact with endocytic dynamins at CCPs.

Next, we explored the role of NM23 NDPK activity in dynamin function. Whereas silencing of both NM23-H1 and -H2 isoforms caused a ~80% decrease of NDPK activity (fig. S8A), overall intracellular GTP levels were not affected by NM23 knockdown (fig. S8B) [nor were other nucleoside triphosphate levels affected (fig. S8C)]. Thus, decreased endocytic rate and increased CCP accumulation of NM23-depleted cells were not a consequence of a reduced bulk intracellular GTP concentration, but rather support a role of NM23-dynamin complexes in which NM23 generates GTP in the vicinity of dynamins to avoid a local drop in GTP/GDP ratio. Indeed, in the absence of added GTP and in the presence of NM23 substrates GDP (1 mM) and ATP (1 mM), catalytically active recombinant NM23-H1 and -H2 proteins triggered GTPase activity of dynamin-1 and -2 (Fig. 3E), whereas kinase-dead NM23-H1^{H118N} mutant did not (Fig. 3E). In the presence of nucleotide concentrations close to cellular levels—100 μM GTP, 10 μM GDP, and 1 mM ATP—NM23-H1 and -H2 were still able to enhance dynamin-1's GTPase activity by 30 to 35%, indicating that NM23 could stimulate dynamin activity further in the presence of physiological GTP level (Fig. 3F). This reflects the capacity of H1/H2 to directly provide GTP to dynamins within NM23/dynamin complexes.

Next, we monitored the capacity of NM23 to promote dynamin-mediated membrane fission in vitro. Classical dynamins can tubulate membrane sheets in the absence of GTP and then fragment the tubules depending on GTP hydrolysis (6). Dynamin-induced tubular networks remained stable in the presence of 1 mM ATP and 1 mM GDP and in the absence of NM23 (Fig. 3G and movie S1), and tubules were not altered by NM23-H1 or -H2 in the absence of nucleotides (Fig. 3G and movies S2 and S3, time 0). In contrast, in the presence of NM23, addition of 1 mM ATP and 1 mM GDP induced breakage and collapse of the tubule network (Fig. 3G and movies S2 and S3), with a fission density of 1 event per 8.3-μm tube length (n = 20 tubes). Most of the fission events occurred during the first 60 s after addition of ATP and GDP (fig. S9A). Immunogold electron microscopy (EM) on liposomes incubated in the presence of purified NM23-H2 and dynamin-1 revealed that NM23-H2 decorated the length of the membrane tubules (Fig. 3, H and I). In addition, EM of negatively stained

preparations of membrane tubules confirmed the association of NM23-H2 to the surface of dynamin-1–coated tubules (fig. S9B). Thus, NM23 bound to membrane-associated dynamin affects dynamin function in membrane fission.

Given the efficiency of NM23-driven GTP supply to dynamins, we explored whether in another compartment, the mitochondria, mitochondrial NM23-H4 isoform was capable of supporting dynamin-related GTPase OPA1. In contrast to the typical tubular morphology of mitochondria in HeLa cells transfected with MitoDsRed, cells silenced for NM23-H4 showed abnormally fragmented and swollen mitochondria (Fig. 4, A and B). Depletion of NM23-H4 phenocopied the loss of OPA1 on mitochondrial morphology, whereas knockdown of NM23-H1/H2 did not alter mitochondrial morphology (Fig. 4, A and B). EM confirmed the severity of mitochondria alterations in NM23-H4–depleted cells (Fig. 4C), which is reminiscent of mitochondrial fusion defects as a result of OPA1 loss of function (19). Furthermore, immunofluorescence staining and PLA documented the colocalization and close proximity of NM23-H4 and OPA1 in mitochondria (Fig. 4D and fig. S10), which is in agreement with their reported interaction (20). To directly show the involvement of NM23-H4 in GTP fueling to OPA1, we determined the GTP hydrolysis rate of OPA1 reflecting GTP loading. Recombinant NM23-H4 triggered OPA1's GTPase activity in the presence of liposomes, mimicking the composition of the mitochondrial inner membrane (Fig. 4E). GTP loading on OPA1 was further increased by ~30% by NM23-H4 in the presence of native mitochondrial GTP concentration (Fig. 4F), which is similar to that observed for NM23-H1/H2 on classical dynamins (Fig. 3F).

We have shown that members of the NM23/NDPK family interact directly and specifically with members of the dynamin superfamily and thus are positioned to maintain high local GTP concentrations and promote dynamin-dependent membrane remodeling. The role of NM23 is well supported by their high NDPK turnover number [k_{cat} 600 s^{-1} per active site (21)]. Furthermore, the localization of the NM23-H3 isoform at the mitochondrial outer membrane (fig. S11), where dynamin Drp1 is recruited to mediate mitochondrial fission, suggests that NM23-H3 could assist Drp1 in this process. These findings identify a general mechanism by which different NDPKs maintain high GTP concentration to high-turnover GTPase dynamins for efficient work in different membrane compartments.

Supplementary Material

Refer to Web version on PubMed Central for supplementary material.

ACKNOWLEDGMENTS

We thank P. De Camilli, E. Smythe, and J. Bertoglio for reagents; S. L. Schmid and M. Mettlen for discussion; the Nikon Imaging Center@Institut Curie & Centre National de la Recherche Scientifique (CNRS) for image acquisition; and I. Hurbain for EM quantification. This work was supported by Institut Curie, CNRS, Fondation ARC pour la Recherche sur le Cancer, Groupement des Entreprises Françaises contre le Cancer, Fondation pour la Recherche Médicale, the Human Frontier Science Program, the Swiss National Fund for Research Grant, and the European Research Council.

REFERENCES AND NOTES

1. Ferguson SM, De Camilli P. Nat. Rev. Mol. Cell Biol. 2012; 13:75–88. [PubMed: 22233676]

2. Schmid SL, Frolov VA. Annu. Rev. Cell Dev. Biol. 2011; 27:79–105. [PubMed: 21599493]
3. Hinshaw JE, Schmid SL. Nature. 1995; 374:190–192. [PubMed: 7877694]
4. Takei K, McPherson PS, Schmid SL, De Camilli P. Nature. 1995; 374:186–190. [PubMed: 7877693]
5. Sweitzer SM, Hinshaw JE. Cell. 1998; 93:1021–1029. [PubMed: 9635431]
6. Roux A, Uyhazi K, Frost A, De Camilli P. Nature. 2006; 441:528–531. [PubMed: 16648839]
7. Morlot S, et al. Cell. 2012; 151:619–629. [PubMed: 23101629]
8. Binns DD, et al. Biochemistry. 2000; 39:7188–7196. [PubMed: 10852717]
9. Marks B, et al. Nature. 2001; 410:231–235. [PubMed: 11242086]
10. Krishnan KS, et al. Neuron. 2001; 30:197–210. [PubMed: 11343655]
11. Dammai V, Adryan B, Lavenburg KR, Hsu T. Genes Dev. 2003; 17:2812–2824. [PubMed: 14630942]
12. Nallamothu G, Woolworth JA, Dammai V, Hsu T. Mol. Cell. Biol. 2008; 28:1964–1973. [PubMed: 18212059]
13. Boissan M, et al. Mol. Cell. Biochem. 2009; 329:51–62. [PubMed: 19387795]
14. Milon L, et al. J. Biol. Chem. 2000; 275:14264–14272. [PubMed: 10799505]
15. Tokarska-Schlattner M, et al. J. Biol. Chem. 2008; 283:26198–26207. [PubMed: 18635542]
16. van der Bliek AM, Shen Q, Kawajiri S. Cold Spring Harb. Perspect. Biol. 2013; 5:a011072. [PubMed: 23732471]
17. Ferguson SM, et al. Dev. Cell. 2009; 17:811–822. [PubMed: 20059951]
18. Praefcke GJ, McMahon HT. Nat. Rev. Mol. Cell Biol. 2004; 5:133–147. [PubMed: 15040446]
19. Griparic L, van der Wel NN, Orozco IJ, Peters PJ, van der Bliek AM. J. Biol. Chem. 2004; 279:18792–18798. [PubMed: 14970223]
20. Schlattner U, et al. J. Biol. Chem. 2013; 288:111–121. [PubMed: 23150663]
21. Lascu I, et al. J. Biol. Chem. 1997; 272:15599–15602. [PubMed: 9188446]

Europe PMC Funders Author Manuscripts

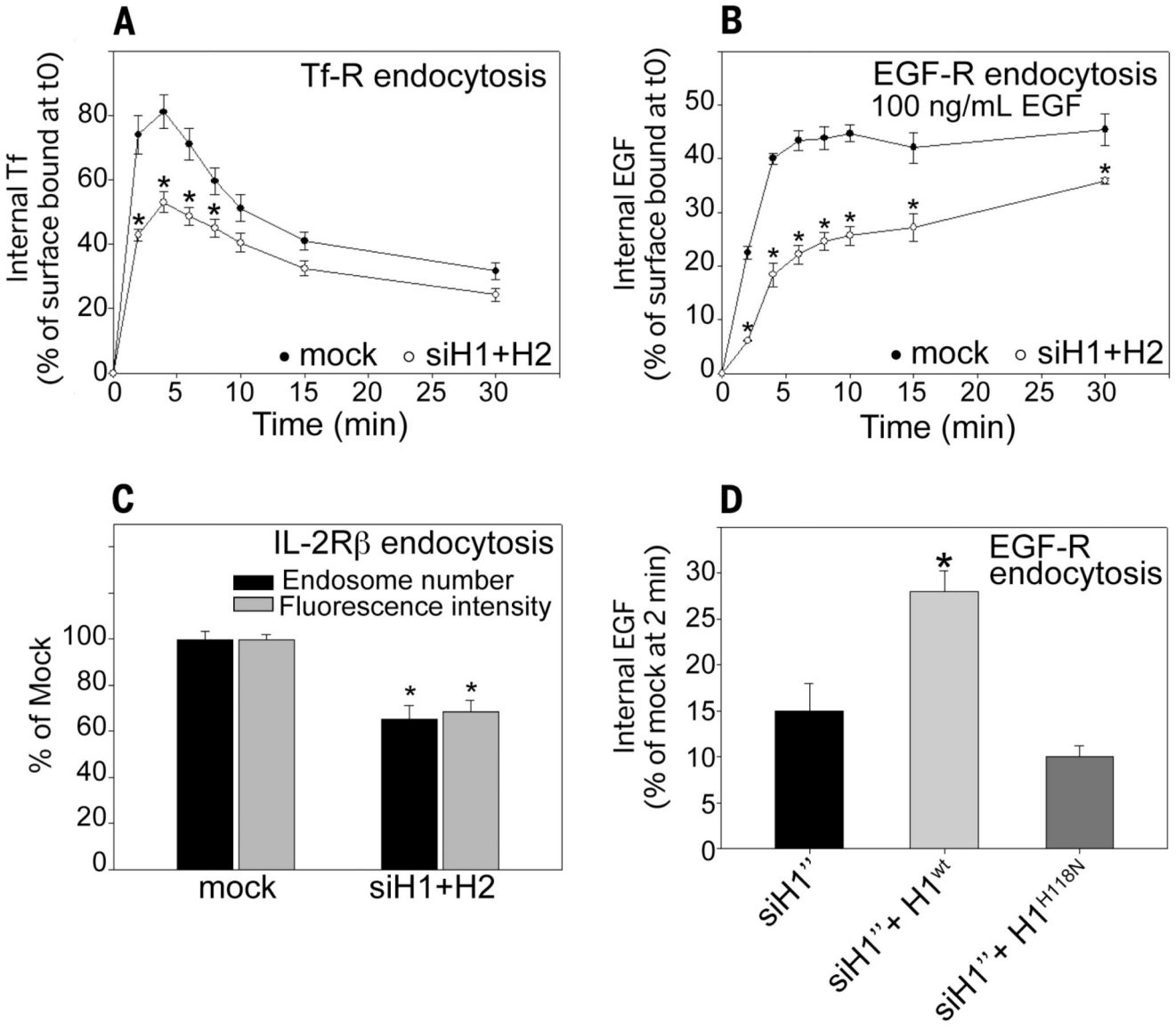

Fig. 1. Nucleoside diphosphate kinases NM23-H1/H2 are required for efficient dynamin-mediated endocytosis

(**A**) HeLa cells were mock-treated or treated with a pair of siRNAs to simultaneously knock down NM23-H1 and NM23-H2 and assessed for endocytosis of Alexa488-Tf. Data are expressed as percentage of internal Tf compared with surface-bound Tf at time 0 ± SEM from four independent experiments. **P* < 0.05 compared with mock-treated cells. (**B**) HeLa cells, either mock-treated or treated with NM23-H1/H2 siRNAs, were assessed for endocytosis of Alexa488-EGF (100 ng/ml). Data are expressed as percentage of internal EGF compared with surface-bound EGF at time 0 ± SEM from four independent experiments. **P* < 0.05 compared with mock-treated cells. (**C**) Hep2 cells stably expressing the interleukin-2 receptor β subunit (IL-2Rβ) were mock-treated or treated with siRNA for NM23-H1/H2 and incubated in the presence of Cy3-coupled antibody to IL-2Rβ for 5 min at 37°C. Data are expressed as average intracellular fluorescence intensity normalized to the

intensity of mock-treated cells ± SEM and endosome number normalized to endosome number in mock-treated cells ± SEM. 100 cells were analyzed from three independent experiments. *$P < 0.05$ compared with mock-treated cells. (**D**) HeLa cells mock-treated or treated with NM23-H1 siRNA were transfected with siRNA-resistant wild-type ($H1^{wt}$) or kinase-dead NM23-H1 ($H1^{H118N}$). EGF endocytosis after 2 min at 37°C was assessed as in (B). *$P < 0.05$ compared with siH1"-treated cells.

Europe PMC Funders Author Manuscripts

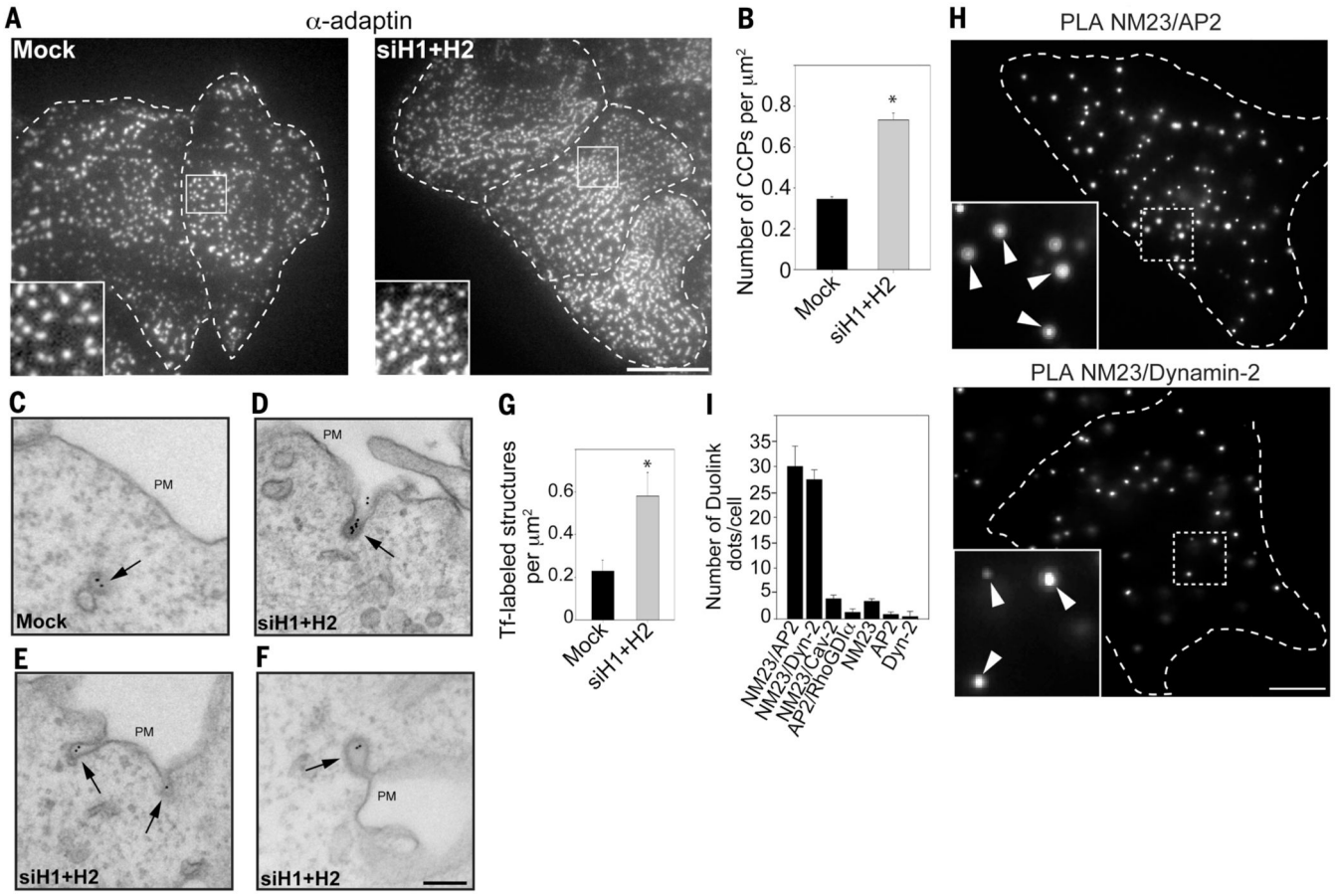

Fig. 2. Accumulation and tubulation of clathrin-coated pits in the absence of NM23-H1/H2

(**A** and **B**) AP-2 staining (α-adaptin) reveals higher CCP density in HeLa cells knocked down for NM23-H1/H2. Scale bar, 5 μm. Graph in (B) represents the mean CCP number/μm^2 ± SEM (n = 10 cells for each condition). *P < 0.05 compared with mock-treated cells. (**C** to **F**) HeLa cells mock-treated (C) or silenced for NM23-H1/H2 [(D) to (F)] were allowed to internalize Tf-Biotin for 4 min at 37°C and analyzed with electron microscopy by means of immunogold labeling with anti-Biotin antibodies and protein-A gold conjugates. Scale bar, 200 nm. (**G**) Number of Tf-positive structures (CCPs and vesicles)/μm^2 in a 1.9 μm-wide region, including the plasma membrane. *P < 0.05 compared with mock-treated cells. (**H**) PLA signal using combination of NM23 and AP-2 (α-adaptin) antibodies (top), or dynamin-2 antibodies (bottom). (Insets) Higher magnification of boxed regions. Scale bar, 5 μm. (**I**) Quantification of PLA dots per cell using different antibody pairs as indicated (mean ± SEM, n = 30 cells/condition from three independent experiments).

Europe PMC Funders Author Manuscripts

Europe PMC Funders Author Manuscripts

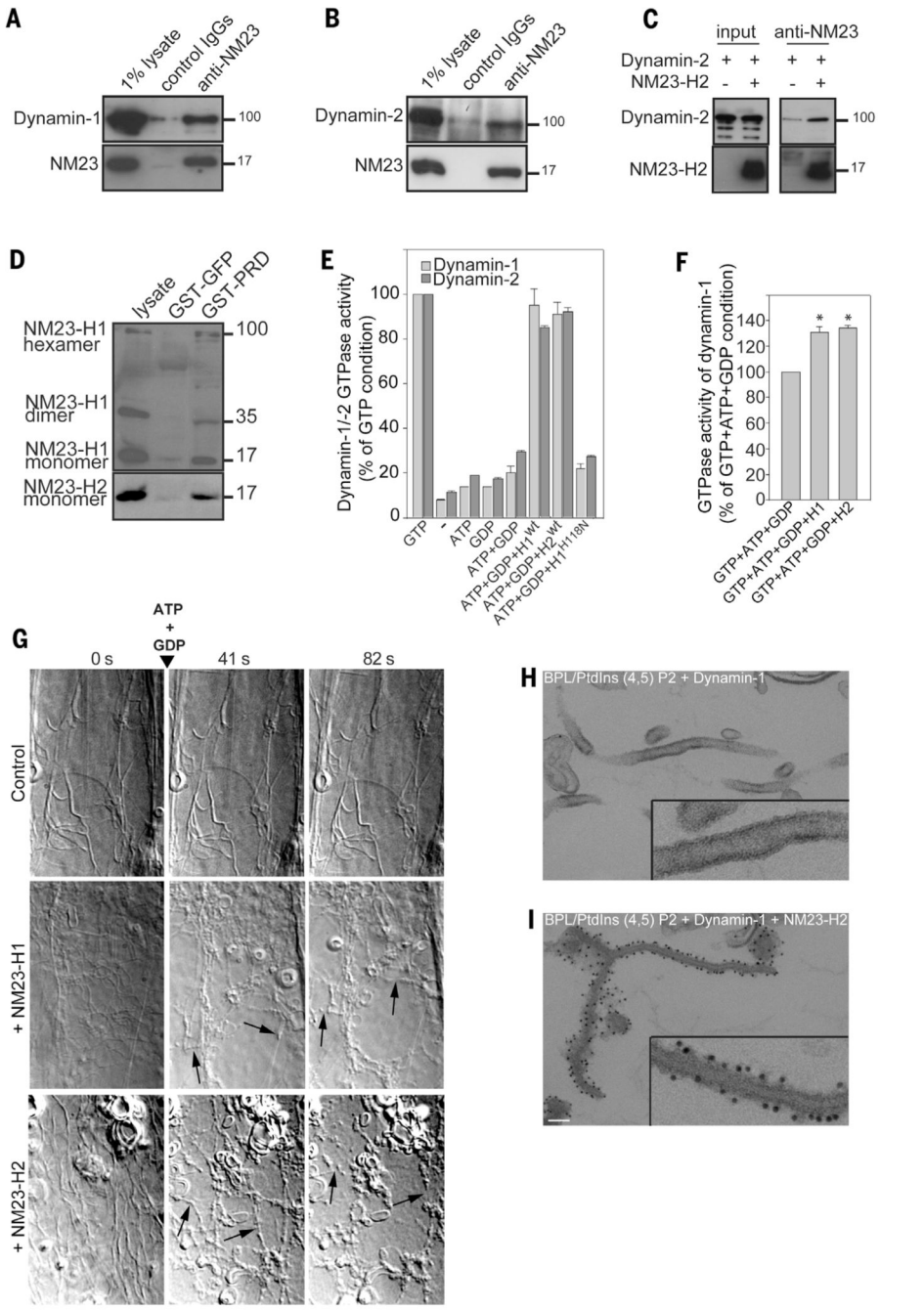

Fig. 3. NM23-H1/H2 promotes dynamin-mediated membrane fission by local GTP regeneration

(**A** and **B**) Lysates of (A) mouse brain or (B) HeLa cells immunoprecipitated with pan–NM23-H1/H2 antibodies and bound proteins analyzed with antibodies to dynamin-1 (A) and -dynamin-2 (B). One percent of total lysate was loaded as a control (input). (**C**) Purified recombinant human NM23-H2 and dynamin-2 were mixed and immunoprecipitated by using antibodies to NM23. Bound proteins were detected with dynamin-2 and NM23 antibodies as indicated. (**D**) Pull-down assays of NM23-H1/H2 from HeLa cell lysates with dynamin-2 GST-PRD or GST-GFP constructs. Bound proteins were detected with specific

antibodies to NM23-H1 and -H2. Monomers and denaturation-resistant dimers and hexamers of NM23-H1 interact with dynamin-2 PRD domain. (**E**) GTPase activity of purified human dynamin-1 and -2 measured in the presence of 95% brain polar lipids (BPL)/5% PtdIns(4,5)P_2 liposomes, recombinant purified wild-type or catalytically dead (H118N) NM23-H1/H2 and nucleotides (1 mM) as indicated. Results are expressed as percentage of controls (1 mM GTP) from triplicate samples from four independent experiments. (**F**) GTPase activity of human dynamin-1 measured as in (E) in the absence or in the presence of NM23-H1 or -H2 and in the presence of physiological nucleotide concentrations (1 mM ATP, 100 μM GTP, and 10 μM GDP). Results are expressed as percent of control condition (ATP+GTP+GDP) from triplicate samples from two independent experiments. *$P < 0.05$ compared with control condition. (**G**) Selected frames from time-lapse sequences showing the effect of purified human NM23-H1/H2 on dynamin-induced membrane tubules after addition of 1 mM ATP and 1 mM GDP. Rat brain dynamin induces tubule formation from the 95% BPL/5% PtdIns (4,5) P_2 liposomes (time 0). Arrows point to tubule fission events in the presence of NM23-H1 or -H2. Representative frames from four independent experiments are shown. (**H** and **I**) Electron micrographs of liposomes incubated (H) with human dynamin-1 alone, which induced tubulation or (I) together with NM23-H2 and stained for NM23 by means of immunogold-labeling. (Insets) Higher magnification. Scale bar, 100 nm.

Europe PMC Funders Author Manuscripts

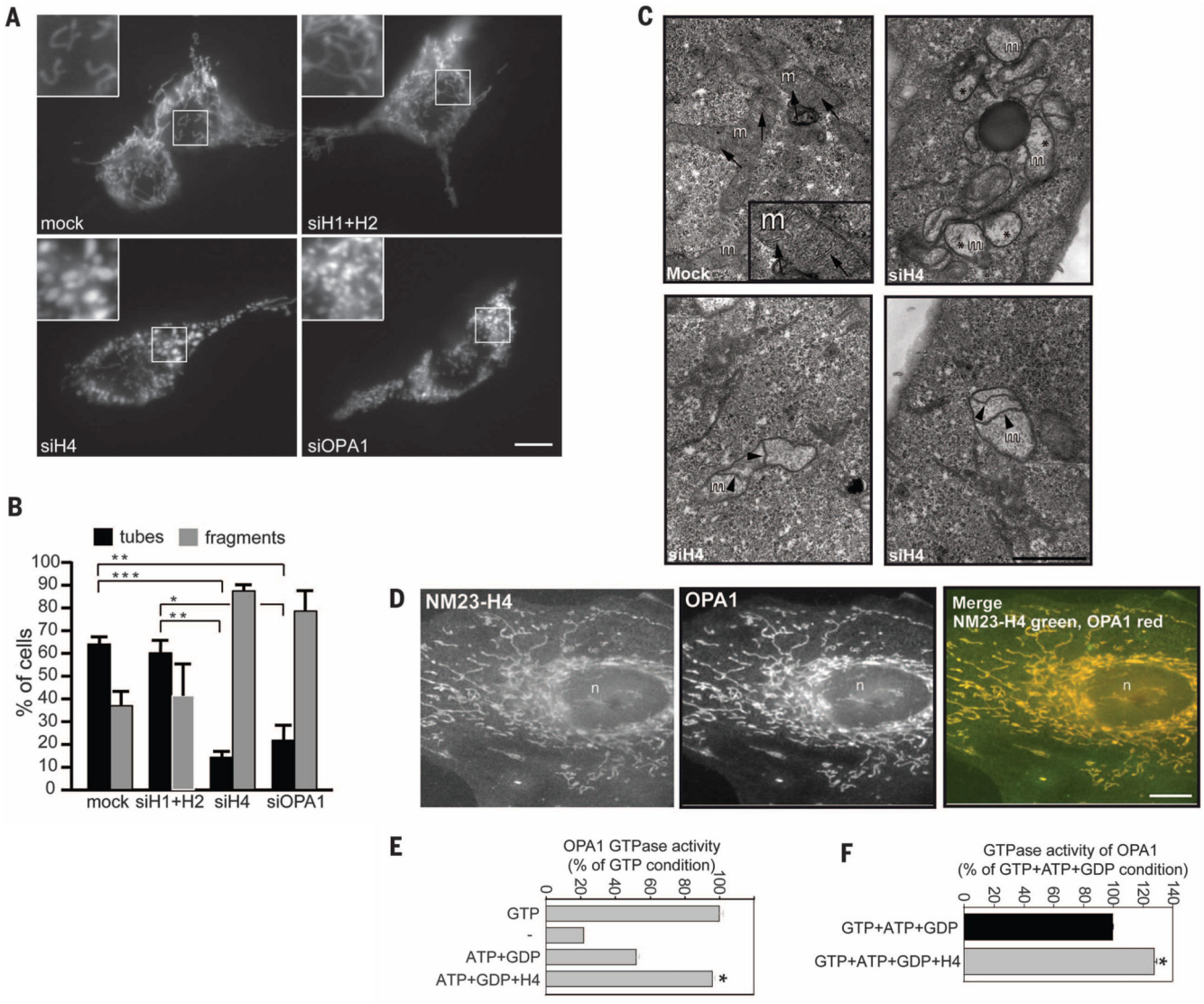

Fig. 4. Mitochondrial NM23-H4 controls mitochondria membrane dynamics through dynamin-related GTPase OPA1

(**A**) HeLa cells transfected with mitochondrial marker mitoDsRED were treated with siRNAs targeting NM23-H1/H2, NM23-H4, or OPA1. Scale bar, 10 μm. (**B**) Percentage of cells with tubular or fragmented mitochondrial morphology in different cell populations as in (A). Mean and SEM are shown for three independent experiments (>100 cells per experiment). ***$P < 0.001$; **$P < 0.01$; *$P < 0.05$. (**C**) EM of HeLa cells silenced for NM23-H4, showing alterations of mitochondrial morphology as compared with that in mock-treated cells. Arrows point to mitochondrial cristae in mock-treated cells. Asterisks indicate mitochondria with loss of cristae and electron-lucent matrix in cells knocked down for NM23-H4. Arrowheads point to internal septae, which appear to divide the inner membrane compartment in H4-KD cells. Scale bar, 1 μm. (**D**) Colocalization of NM23-H4 and OPA1 in mitochondria in HeLa cells. Scale bar, 10 μm. (**E**) GTPase activity of purified recombinant human OPA1 measured in the presence of 25% cardiolipin-enriched liposomes and purified NM23-H4 as in Fig. 3E. Results are expressed as percentage of control

condition (1 mM GTP) from three independent experiments. *$P < 0.05$ compared with the ATP+GDP condition. (**F**) GTPase activity of human OPA1 in the presence of cardiolipin-enriched liposomes and NM23-H4 measured in the presence of physiological mitochondrial nucleotide concentration (1 mM ATP, 100 μM GTP, and 10 μM GDP). Results are expressed as percent of control (ATP+GTP+GDP) from duplicate samples from two independent experiments. *$P < 0.05$ compared with the control condition.

Europe PMC Funders Author Manuscripts